



ELSEVIER

Journal of Electron Spectroscopy and Related Phenomena 70 (1995) 197–206

JOURNAL OF
ELECTRON SPECTROSCOPY
and Related Phenomena

Angular resolved autoionization spectroscopy of N₂ on Ni(110)

N. Sauerwald, J. Klinkmann, T. Porwol, G. Dömötör, I. Hemmerich, H.-J. Freund*

Lehrstuhl für Physikalische Chemie I, Ruhr-Universität Bochum, Universitätsstrasse 150, D-44780 Bochum, Germany

First received 30 March 1994; in final form 27 May 1994

Abstract

Angular resolved autoionization spectra after core to bound excitation of N₂ adsorbed on Ni(110) are presented. The experimental autoionization spectra are compared with calculated spectra for the model system Ni–N–N by application of the many-body Green's function technique using SCF–MO–CNDO one particle wavefunctions. The angular dependences of the autoionization lines are explicitly calculated. The theoretical approach allows one to assign the spectra obtained after core to bound excitation including angular effects within the framework of molecular orbital theory. The assignment is compared with results for the CO on Ni(110) system.

Keywords: AES; Autoionization; CNDO; LEED; Ni(110); Nitrogen

1. Introduction

The system N₂/Ni(110) is of great interest because N₂ is a reactant for several important technical processes and comprises an example of "weak" chemisorption [1–6]. One of the most powerful techniques used to characterize the electronic structure of adsorbate systems is photoelectron spectroscopy [7–10]. Because photoionization is a complex dynamic many particle process, it is not possible to observe the binding energy of the electrons in the ground state directly; for this it would be necessary that no relaxation of the orbitals in the ion state took place.

However, due to the strong relaxation of the ions a complex pattern of single hole and satellite states is observed. This phenomenon is called breakdown of Koopmans' theorem [11–13]. The satellites "borrow" their intensity from the single hole states in the inner valence region [14,15]. For this reason and the strong secondary electron emission,

it is difficult to resolve the satellite states spectroscopically. In contrast to PES the states are "directly" populated via the autoionization process. In the present work, the autoionization of adsorbed nitrogen on the Ni(110) surface is studied experimentally and the results are compared with theoretical calculations.

The model system used for the calculations in this study is a linear Ni–N–N cluster. With this theoretical model we are able to explain the experimental results within the framework of molecular orbital theory. In particular, the angular dependences of the experimental autoionization spectra are compared with the angular dependences of the transition rates determined by calculation.

2. Theoretical considerations

For the theoretical treatment of the autoionization process a Green's function formalism was applied

[16–18]. We used both ab initio and semiempirical wave functions of the model system Ni–N–N. The semiempirical method employed was the complete neglect of differential overlap (CNDO) method. For the ab initio calculations the program CADPAC 4.2 was used which was installed on the Cray Y-MP of the Forschungszentrum Jülich. It is well known that CNDO eigenvalues are shifted to higher binding energies by 3 to 5 eV [19]. These values enter directly into the Dyson equation resulting in relatively high binding energies for the satellite states (2 hole 1 particle (2h1p)). The satellite states cannot be shifted to lower binding energies because of a singularity in the real part of the self energy. Therefore, in this work we have used the eigenvalues obtained by the ab initio calculations. For these calculations a basis set published by Ohno and von Niessen [20] was used which is an extended Wachters set [21] for the nickel atom and a basis set of Salez and Veillard [22] for the nitrogen. This cluster has a linear geometry because each nitrogen molecule sits perpendicularly to the surface on top of a nickel atom in the case of Ni(110) [10,23] as well as Ni(100) [24]. Two different sets of parameters were used for our calculations. The internal distances $d_{\text{Ni-N}} = 1.82 \text{ \AA}$ and $d_{\text{N-N}} = 1.13 \text{ \AA}$ which are equivalent to those in the Ni(CO)₄-complex and well known from the literature [17] and a cluster with $d_{\text{Ni-N}} = 1.64 \text{ \AA}$ and $d_{\text{N-N}} = 1.10 \text{ \AA}$ which are the parameters used by Ohno and von Niessen [20] were used for comparison. The results presented are calculated using the first cluster because there was only a small difference in the overall dependence of the calculated values by varying the bond length.

The description of the autoionization spectra is as follows. The probability of a population of a special state is described as

$$I_{ab} \propto \sum_{l,m} |\langle \Psi_{\text{ion}}^b e^{l,m} | \hat{\mathcal{H}} | \Psi_{\text{neutral}}^a \rangle|^2 \quad (1)$$

Ψ_{neutral}^a represents the initial state which is the highly excited neutral state after the core to bound excitation; Ψ_{ion}^b is the final state after the radiationless decay of the initial state, and $e^{l,m}$ represents the leaving electron. $\hat{\mathcal{H}}$ is the Hamiltonian for the described process. The initial state

wave function is approximated as

$$|\Psi_{\text{neutral}}^a\rangle \approx |\phi_{1s \rightarrow \pi^*}\rangle \quad (2)$$

i.e. a single determinant representation was chosen for the core to bound excited neutral state. Technically this was done in the equivalent core approximation [25]. For this system configuration interaction effects were omitted because they are of negligible importance. This conclusion was drawn from the narrow π resonance in the near-edge X-ray adsorption fine structure (NEXAFS) spectrum. This simplification is not possible in the description of the final state wave function. In terms of configuration interaction it has to be described as

$$|\Psi_{\text{ion}}^b e^{l,m}\rangle \approx |\hat{A} \sum_{l,m} \sum_{\mu} c_{\mu b} |\phi_{\mu}\rangle \psi_{l,m}\rangle \quad (3)$$

where \hat{A} represents the antisymmetrizer, $\psi_{l,m}$ are spherical waves centered at the core hole site characterized by a set of angular momentum quantum numbers (l, m), describing the emitted electron. The index μ in Eq. (3) enumerates the possible final state configurations of the ion state CI eigenvectors obtained by the Green's function calculation. Within this approximation the intensity is given as

$$I_{ab} = \sum_{l,m} \sum_{\mu,\nu} c_{\mu,b}^* c_{\nu,b} \langle \hat{A} \phi_{\mu} \psi_{l,m} | \hat{\mathcal{H}} | \phi_i \rangle \times \langle \phi_i | \hat{\mathcal{H}} | \hat{A} \phi_{\nu} \psi_{l,m} \rangle \quad (4)$$

Introducing the abbreviation

$$M_{\mu}^{l,m} = \langle \phi_i | \hat{\mathcal{H}} | \hat{A} \phi_{\mu} \psi_{l,m} \rangle \quad (5)$$

it is possible to write

$$I_{ab} = \sum_{l,m} \sum_{\mu,\nu} c_{\mu,b}^* c_{\nu,b} M_{\mu}^{l,m*} M_{\nu}^{l,m} \quad (6)$$

The doublet states originating from the autoionization process may be classified according to four different types under the assumption that the ground state of the molecule is $^1\Sigma$. The first possibility is a relaxation where the spectator electron is taking part. The corresponding state is a single hole state. The matrix elements are a combination of integrals of the type

$$V_{1s\psi\pi^*i} = \langle \phi_{1s}(1) \psi_{l,m}(2) | \frac{1}{r_{12}} | \phi_{\pi^*}(1) \phi_i(2) \rangle \quad (7)$$

In the case of a single hole state one can write [26,27]

$$M^{l,m} = 2V_{1s\psi ij} - V_{1s\psi i\pi^*} \quad (8)$$

For the 2h1p configurations one has to calculate the matrix elements

2hp (singlet coupled) ($i < j$)

$$M^{l,m} = \frac{1}{\sqrt{2}}(V_{1s\psi ij} + V_{1s\psi ji}) \quad (9)$$

2hp (triplet coupled) ($i < j$)

$$M^{l,m} = \frac{\sqrt{3}}{\sqrt{2}}(V_{1s\psi ij} - V_{1s\psi ji}) \quad (10)$$

2hp (both holes in the same spatial orbital) ($i = j$)

$$M^{l,m} = V_{1s\psi ii} \quad (11)$$

The mode of coupling depends on the state of the molecule without the spectator. The integrals are expanded in the one-center approximation proposed by Siegbahn et al. [28]

$$J_{l,m} = \langle \phi_i(1)\phi_j(2) \left| \frac{1}{r_{12}} \right| \phi_{1s}\psi_{l,m}(2) \rangle \quad (12)$$

$$= \sum_{r,s} c_r^i c_s^j \langle \chi_i(1)\chi_j(2) \left| \frac{1}{r_{12}} \right| \phi_{1s}(1)\psi_{l,m}(2) \rangle \quad (13)$$

$$= \sum_{l',m'} \sum_{l'',m''} c_{l',m'}^i c_{l'',m''}^j \delta(m' + m'', m) \\ \times \sum_k c^k(l', m', 00) c^k(lm, l''m'') \\ \times R^k(nl', nl'', 0l) \quad (14)$$

Here the terms $c_{l',m'}^{i,j}$ mean the LCAO expansion coefficients of the SCF calculation, $c^k(l', m', 00)$ are Clebsh Gordon coefficients, and $R^k(nl', nl'', 0l)$ the radial integrals of McGuire [29,30]. To study the angular dependence of the autoionization spectra, we consider the final state wave function Ψ_F as [31]

$$\Psi_F = 4\pi \sum_{l,m} i^l \exp(i\beta_l) Y_{l,m}^*(\vec{k}) Y_{l,m}(\vec{r}) G_{kl}(r) \quad (15)$$

where \vec{k} is the unit vector pointing in the direction of the outgoing electron, $G_{kl}(r)$ represents the radial part of the wave function and β_l is the phase factor of the l th partially scattered

wave. The complete intensity has now to be written as

$$I_{ab}(\theta) = \sum_{l,m} \sum_{\mu,\nu} c_{\mu b}^* c_{\nu b} M_{\mu}^{l,m*} M_{\nu}^{l,m} Y_{l,m}^*(\theta, \phi) \\ \times Y_{l,m}(\theta, \phi) \quad (16)$$

The further procedure has been published elsewhere [26,32].

3. Experimental procedure

The experiments were performed in a magnetically shielded (double μ -metal shield) vacuum system containing facilities for low energy electron diffraction (LEED), Auger electron spectroscopy (AES), residual gas analysis with a quadrupole mass spectrometer, and an angle resolved hemispherical photoelectron detector (VSW HA 50). The measurements were carried out at the BESSY I storage ring [37] on the high energy toroidal grating monochromator 2 (HE-TGM 2). The base pressure in the system was below 1×10^{-9} mbar.

The Ni(110) crystal was spot welded to two tungsten rods mounted on a sample manipulator. The sample could be cooled with liquid nitrogen to 80–85 K. Heating was achieved via electron bombardment from a filament on the reverse side of the crystal.

The surface of the crystal was cleaned by argon ion bombardment, followed by annealing. Nitrogen adsorption was performed by cooling the sample to $T = 80$ –85 K followed by dosing with 31N_2 . Only after annealing to 125 K could an ordered (2×1) structure be observed [4]. The preparation is difficult and had to be repeated very frequently to obtain the desired LEED pattern.

To determine the angular dependence, we used a fitting procedure to obtain the areas under each peak. Because the number of states is too large to fit a distribution of one curve for every state, groups of states were summed together to form peaks to be fitted. The energy position of those peaks was determined from the experiment. A peak was fitted whenever a structure in one of the spectra at different polar angles was observed. This is the reason that 12 Student t distributions

have been fitted. These curves were fitted to each of the spectra at identical positions with the same full width at half maximum and using the same functional form. To solve the fitting problem a new routine was programmed to obtain optimal results for every angle. We developed a two-dimensional simplex algorithm fitting all of the spectra at the same time, obeying the boundary conditions described before [23]. In this way it was possible to optimize the localization and shape of the distributions.

4. Results and discussion

The autoionization spectrum of $N_2(2 \times 1)/Ni(110)$ and the photoelectron spectrum of clean nickel are shown in Fig. 1. The autoionization spectrum is dominated by four intense features in addition to emission from the d band. The first feature is located at about 13 eV. The second is the most intense and is located at 21 eV binding energy. The third maximum at about 27 eV, in energy directly above the major peak, is followed by the fourth structure which is a broad peak at about 42 eV. It is obvious that not each of these spectral features represents single states.

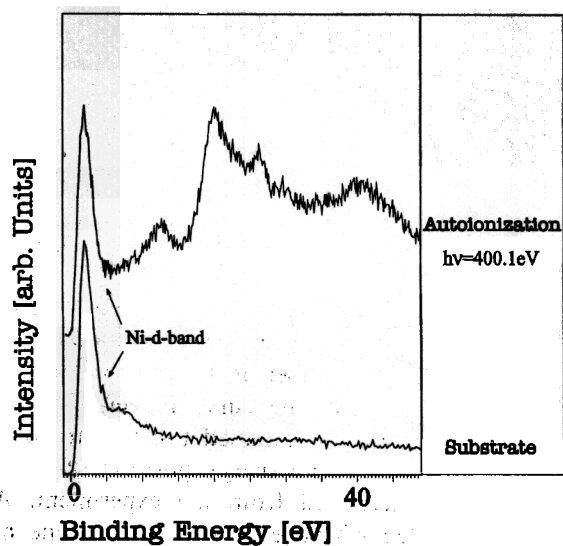


Fig. 1. Series of photoelectron spectra and autoionization spectra.

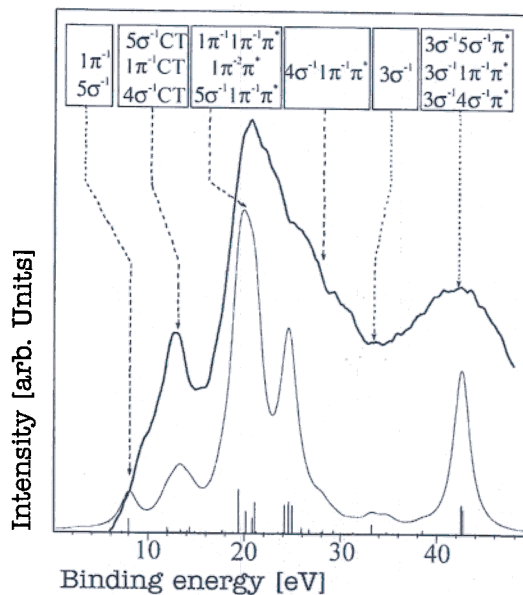


Fig. 2. Comparison between the calculated and measured autoionization spectra. The calculated line spectrum has been convoluted with a Lorentzian line of 2 eV FWHM.

Therefore, a more detailed and theoretical model of the process and the system is needed. Its theoretical background has been summarized in Section 2 and is discussed elsewhere [32].

The measured autoionization spectrum after background subtraction and the calculated spectrum are shown in Fig. 2. The latter was obtained by convoluting the calculated states with Lorentzian functions of 2 eV full width at half maximum. The calculated spectrum has been shifted by about 7 eV (about 5 eV workfunction of the surface [10]) to lower binding energies. The general features of the autoionization spectrum are very well reproduced by our simplified model.

For a first overview it is not necessary to consider the exact assignments of the individual lines. Rather we consider distinct transition regimes. The first one is situated at energies lower than 10 eV. It contains the single hole states of the 5σ - and 1π -orbital. The second regime, at around 13 eV, contains states which are formed when a metal orbital ($M\pi$) takes part in the relaxation process. Those screened states of the type ($\dots M\pi^{-1}\pi^*$) are referred to as charge transfer (CT) states below. The most intense feature in the

Table 1
Autoionization matrix elements for pure configurations^a

Intensities		Ground state		Final state
Equivalent core approximation		Ground state		
Outer	Inner	Outer	Inner	
0.234	0.281	0.127	0.144	(3σ ⁻² π*)
0.297	0.358	0.215	0.267	(3σ ⁻¹ 4σ ⁻¹ π*) ¹
0.029	0.049	0.017	0.027	(3σ ⁻¹ 4σ ⁻¹ π*) ³
0.222	0.271	0.139	0.162	(3σ ⁻¹ 1π ⁻¹ π*) ¹
0.046	0.057	0.024	0.029	(3σ ⁻¹ 1π ⁻¹ π*) ³
0.222	0.271	0.139	0.162	(3σ ⁻¹ 1π ⁻¹ π*) ¹
0.046	0.057	0.024	0.029	(3σ ⁻¹ 1π ⁻¹ π*) ³
0.176	0.099	0.231	0.137	(3σ ⁻¹ 5σ ⁻¹ π*) ¹
0.033	0.020	0.036	0.024	(3σ ⁻¹ 5σ ⁻¹ π*) ³
0.043	0.004	0.017	0.000	(3σ ⁻¹ Mπ ⁻¹ π*) ¹
0.043	0.004	0.017	0.000	(3σ ⁻¹ Mπ ⁻¹ π*) ¹
0.121	0.217	0.090	0.134	(4σ ⁻² π*)
0.225	0.361	0.124	0.192	(4σ ⁻¹ 1π ⁻¹ π*) ¹
0.021	0.019	0.019	0.021	(4σ ⁻¹ 1π ⁻¹ π*) ³
0.225	0.361	0.124	0.192	(4σ ⁻¹ 1π ⁻¹ π*) ¹
0.021	0.019	0.019	0.021	(4σ ⁻¹ 1π ⁻¹ π*) ³
0.204	0.182	0.206	0.178	(4σ ⁻¹ 5σ ⁻¹ π*) ¹
0.043	0.005	0.015	0.000	(4σ ⁻¹ Mπ ⁻¹ π*) ¹
0.043	0.005	0.015	0.000	(4σ ⁻¹ Mπ ⁻¹ π*) ¹
0.280	0.358	0.161	0.200	(1π ⁻² π*)
0.352	0.452	0.203	0.252	(1π ⁻¹ 1π ⁻¹ π*) ¹
0.229	0.157	0.230	0.174	(1π ⁻¹ 5σ ⁻¹ π*) ¹
0.108	0.010	0.039	0.000	(1π ⁻¹ Mπ ⁻¹ π*) ¹
0.068	0.007	0.025	0.000	(1π ⁻¹ Mπ ⁻¹ π*) ¹
0.280	0.358	0.161	0.200	(1π ⁻² π*)
0.229	0.157	0.230	0.174	(1π ⁻¹ 5σ ⁻¹ π*) ¹
0.068	0.007	0.025	0.000	(1π ⁻¹ Mπ ⁻¹ π*) ¹
0.108	0.010	0.039	0.000	(1π ⁻¹ Mπ ⁻¹ π*) ¹
0.114	0.043	0.195	0.093	(5σ ⁻² π*)
0.044	0.002	0.028	0.000	(5σ ⁻¹ Mπ ⁻¹ π*) ¹
0.044	0.002	0.028	0.000	(5σ ⁻¹ Mπ ⁻¹ π*) ¹
0.010	0.000	0.002	0.000	(Mπ ⁻² π*)
0.013	0.000	0.003	0.000	(Mπ ⁻¹ Mπ ⁻¹ π*) ¹
0.010	0.000	0.002	0.000	(Mπ ⁻² π*)
0.159	0.191	0.203	0.217	3σ ⁻¹
0.101	0.124	0.169	0.195	4σ ⁻¹
0.105	0.131	0.139	0.156	1π ⁻¹
0.105	0.131	0.139	0.156	1π ⁻¹
0.060	0.035	0.164	0.091	5σ ⁻¹
0.020	0.002	0.017	0.000	2π ⁻¹
0.020	0.002	0.017	0.000	2π ⁻¹

^a Superscripts 1/3 indicate singlet/triplet coupled doublet final states, respectively. 2h1p configurations without a superscript are singlet coupled doublet final states with both holes residing in the same spatial orbital.

18–22 eV energy range is comprised of four states with large intensities originating from configurations of the form (1π⁻¹X⁻¹π*)¹ where X can be 1π or 5σ. The next peak in the range 23–30 eV stems from (4σ⁻¹1π⁻¹π*)¹ or ³ states. Again, the 1π orbital plays a dominant role. The very small feature at 33 eV is due to the 3σ single hole state, whose satellites (3σ⁻¹1π⁻¹π*) give rise to the last peak in the theoretical spectrum situated at 40–50 eV.

Table 1 shows the calculated intensities of the pure configurations, i.e. without configuration interaction. Here the results are the same as published before [26,32]. The (1π⁻²π*), the (1π⁻¹1π⁻¹π*) and the (1π⁻¹5σ⁻¹π*) states give

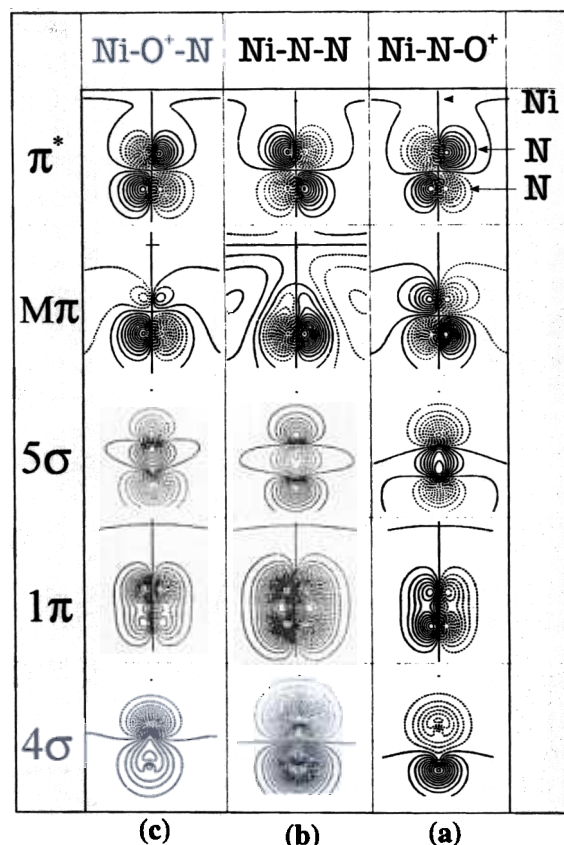


Fig. 3. Relative densities of electrons before (panel b) and after core to bound excitation of the outer (panel a) and the inner nitrogen (panel c). The densities shown are calculated at the CNDO level.

rise to the largest intensities. Since Ni–N–N has two chemically inequivalent nitrogen atoms, we have performed two separate calculations. The theoretical results shown in Fig. 2 are a superposition of both spectra. In our experimental work, it has not been possible to resolve the two different contributions (see, however, the work by the Uppsala group [33,34]).

In order to qualitatively interpret the results we remember that an important factor for determining the size of the matrix elements, i.e. the intensity, is the degree of overlap between the π^* orbital, the valence, and the 1s orbitals. We have plotted the orbitals of the different nitrogen atoms in the equivalent core approximation in Fig. 3. It is clear from the diagram that the electron density at the site of the excited nitrogen atom depends on the final orbital. For example it is larger for the inner nitrogen atom in the case of the 1π decay and for the outer atom in the case of the decay into the 5σ and the $M\pi$ orbitals. The direct conclusion from this finding is that ion states with a high degree of participation of the 1π orbital have a higher intensity for excitation of the inner atom, and states with a high degree of participation of the 5σ or $M\pi$ orbital have a higher intensity for excitation of the outer nitrogen atom. Furthermore, the overall intensity should be slightly higher after excitation of the inner than of the outer nitrogen atom. Table 2, which shows the assignment of the most intense states in the spectra, verifies this conclusion.

Björneholm et al. [33,34] succeeded in resolving

Table 2
Assignment of the autoionization spectra

$E_{\text{Bin}}^{\text{a}}$	Assignment	Angular dependence ^c
9.3		(+)
12.7		(+)
16.8		+
19.9		+
24.2		(+)
26.5		(+)

^a With reference to E_f . ^b CT, decay with metal orbital taking part. ^c +, Angular dependence fits very well; (+), angular dependence is interpretable.

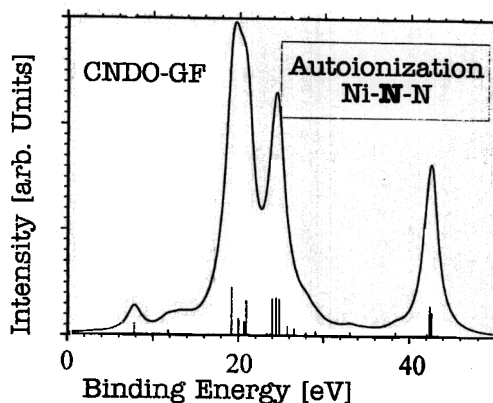


Fig. 4. Calculated autoionization spectrum after $N1s \rightarrow \pi^*$ excitation of the inner nitrogen atom. The line spectrum has been convoluted with a Lorentzian line of 2 eV FWHM.

the autoionization spectra of the two chemically different nitrogen atoms of N_2 on Ni(100). They fitted the NEXAFS resonance with two peaks for the two chemically different nitrogen atoms and took autoionization spectra of the outer nitrogen at 399.4 eV and one with an increased contribution of the inner nitrogen at 401.0 eV. Their autoionization spectra agree well with ours for the $N_2/Ni(110)$ system. In addition, it is possible to model the spectra with our calculations. An interesting fact is that the CT states at about 13 eV appear in the spectrum of the outer and disappear in the spectrum of the inner nitrogen. Björneholm et al. [33] point out that one reason for this

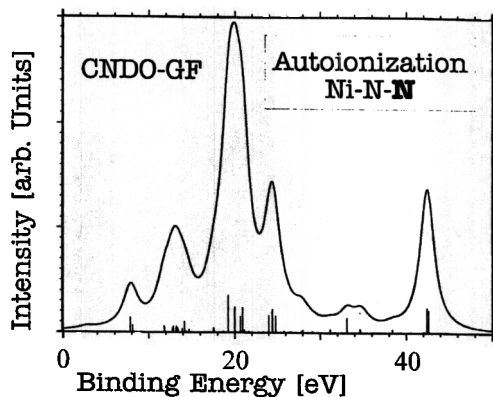


Fig. 5. Calculated autoionization spectrum after $N1s \rightarrow \pi^*$ excitation of the outer nitrogen atom. The line spectrum has been convoluted with a Lorentzian line of 2 eV FWHM.

might be the much stronger π^* -Ni3d hybridization of a “NiNO”-like state than of a “NiON” state. Our calculations also verify this result. The calculated spectra for the different nitrogen atoms are shown in Figs. 4 and 5. The peak at 25 eV which disappears in the spectrum of the inner nitrogen is not modeled very well in our calculation because it is larger in the autoionization of the inner than in that of the outer nitrogen.

It is our experience that the agreement of the calculations with experiment decreases with increasing binding energy which results from the use of the 2ph-Tamn-Dancoff approximation in the Green’s functions calculation. In the higher energy region, 3h1p states and other higher excited states contribute to the spectra but are not taken into account in the calculations. In spite of this difficulty we have been able to obtain good overall agreement between our crude model and the measurements.

Another proof for the validity of our model is from the calculation of the angular dependence of the spectrum. It is not difficult to understand qualitatively that there must be an angular dependence of the autoionization intensities [35,36]. The contributing matrix elements are of the form [28]

$$\langle \Psi_i \Psi_j | \frac{1}{r_{12}} | \Psi_k \Psi_{l,m} \rangle$$

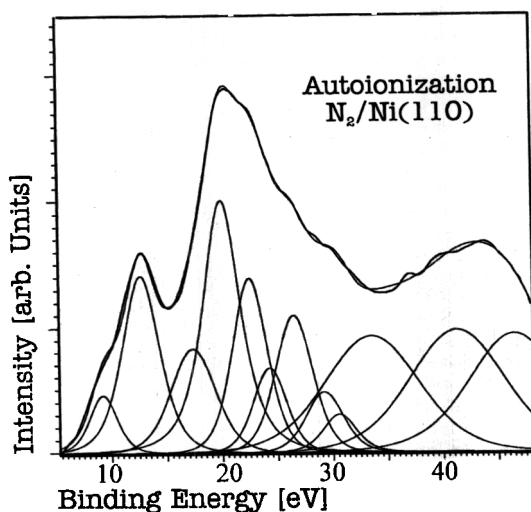


Fig. 6. Measured spectrum with fitted Student t distributions.

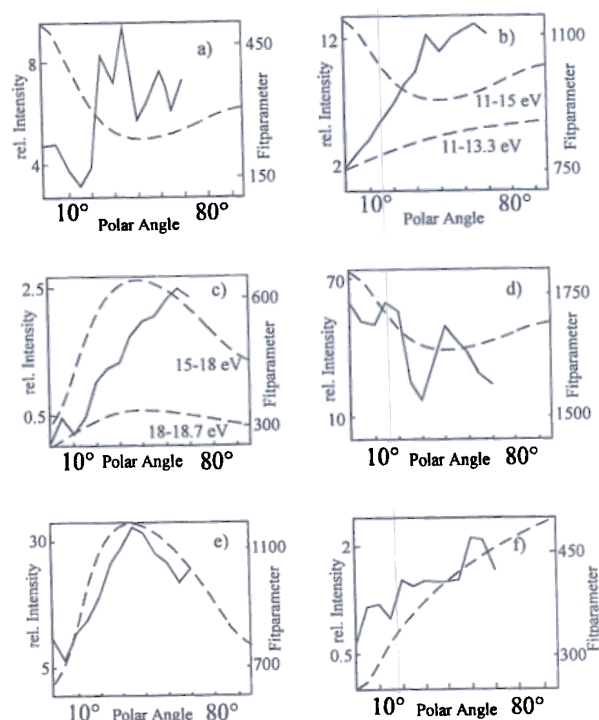


Fig. 7. Relative intensities of the spectral features centered at the given binding energies of the N1s $\rightarrow \pi^*$ decay spectrum as a function of polar angle.

where $\Psi_{l,m}$ is the wave function for the emitted electron and Ψ_i , Ψ_j and Ψ_k represent the wave functions of the participating orbitals in the decay process. To obtain a nonvanishing intensity, the whole matrix element must contain the totally symmetric representation σ^+ which is also the representation of the coulomb operator. The symmetry of $\Gamma_i \times \Gamma_j \times \Gamma_k$ is determined by the selection of the state to be populated. So the symmetry condition is

$$\Gamma_i \times \Gamma_j \times \Gamma_k \times \Gamma_{\hat{O}p} \times \Gamma_{l,m} \subset \sigma^+$$

The exact angular dependence is strongly determined by the orbitals i, j, k which has been taken into account in the calculations as described before. The spectra have been measured in steps of 5° of the polar angle and show an angular dependence. The azimuthal angular dependence has been shown in other experiments (CO/Ni(110) [32]) to be not very pronounced and is not taken into account.

The results of the fitting procedure described in Section 2 are shown for the angle integrated spectrum in Fig. 6. Figure 7 shows the results of the angular dependence in the experiment and the calculations for eight peaks. Peaks 9–12 are only necessary to model the high energy range of the spectra and will not be addressed further.

The first experimental peak is located at 9.3 eV. The states in the calculations between 7 and 11 eV are considered. In this region the intensity is dominated by the three single hole states $5\sigma^{-1}$, $1\pi^{-1}$ and $4\sigma^{-1}$. The experimental dependence of angle is not very significant and is very similar for the pure configurations $5\sigma^{-1}$ and $4\sigma^{-1}$ while the calculation is dominated by the $1\pi^{-1}$ angular dependence. We may say that the intensity of the $1\pi^{-1}$ state is estimated to be too high in the calculations. With a lower contribution for that state we can obtain the experimental curve almost exactly because for low angles the $1\pi^{-1}$ state creates some intensity but the maximum is determined from the $5\sigma^{-1}$ and $4\sigma^{-1}$ states at about 40 to 50° (Fig. 7(a)).

The second distribution is situated at 12.7 eV. Therefore the states from 11 to 15 eV are summed. This region is governed by the charge transfer satellites of the 1π and 5σ orbitals. The charge transfer satellites of the 4σ orbital dominate the next peak. The angular dependence does not fit very well with the experimental values. The three most intense features between 13.3 and 15 eV have a maximum at 0° and a minimum at about 40°. If only the states situated between 11 and 13.3 eV are taken into account, the angular dependence is compatible (Fig. 7(b)).

The third distribution contains, as mentioned before, the CT satellites of the 4σ orbital. This region is centered at 17.4 eV. The states from the theoretical spectra which represent this feature are in the energy region from 15 to 18.7 eV. As can be seen in Fig. 7(c) the angular dependence of the calculated and the experimental data agree very well.

The fourth distribution is governed by the most intense features of the whole spectrum and also possesses the largest intensity in the experimental data. It is centered at 20 eV and is totally dominated by three states. The highest transition rate is given by the $(1\pi^{-1}1\pi^{-1}\pi^*)^1$ state. This is a singlet coupled state having two holes in two “different”

1π orbitals. The next intense state is a $(1\pi^{-2}\pi^*)$ state. Here, in contrast to the previous state, both holes are located in the same spatial 1π orbital. The cluster which is used has $C_{\infty v}$ symmetry making both 1π orbitals equivalent. On the surface the symmetry is reduced, so the two 1π derived orbitals are not necessarily equivalent any more. For this reason we have differentiated the two 1π states. The third state is of $(1\pi^{-1}5\sigma^{-1}\pi^*)^1$ type. The ratio of the calculated transition probabilities of the three is 2.8:2:1. The angular dependence of these features is represented very well by the calculation. The maximum at 0° is totally governed by the $(1\pi^{-2}\pi^*)$ state while the $(1\pi^{-1}1\pi^{-1}\pi^*)^1$ is responsible for the ascendance after the minimum at about 45°. The contribution of $(1\pi^{-1}5\sigma^{-1}\pi^*)^1$ results in the minimum being less deep (Fig. 7(d)). From this information, one has to say that the most intense feature of the spectrum consists of satellites with participation from the 1π orbitals.

The fifth, sixth and seventh distributions are shown in Fig. 7(e). The intensity of these peaks is given by $(4\sigma^{-1}1\pi^{-1}\pi^*)^1$ configurations. The three distributions have a large overlap so that the description of the angular dependence is difficult to obtain. They are placed at 22.5, 24.7 and 26.4 eV. The angular dependence of the whole region fits very well with the angular dependence of the fifth distribution. However, there is no correspondence with the sixth and seventh distributions. The angular dependence of the sixth distribution is weak.

The seventh distribution is intense and has a strong angular dependence. This angular dependence fits with the $(5\sigma^{-2}\pi^*)$ state but this state has no significant intensity. As mentioned before, this region is modeled very well in comparison with the data of Björneholm et al. [33].

The eighth distribution at 29.21 eV is governed by states of the $(4\sigma^{-1}1\pi^{-1}\pi^*)^3$ type. The angular dependence fits very well with the calculated dependence as shown in Fig. 7(f). The ninth distribution is located at 30.6 eV. The angular distribution of this peak is difficult to interpret because there is a large overlap with the following distributions.

In summary, there is qualitative agreement between the experimental and calculated angular

Table 3
Assignment of the spectra

This work		Björneholm et al. ^d	
E_{Bin}^a	Assignment	$E_{\text{Kin(Bin)}}^{a,b}$	Assignment
9.3	$5\sigma^{-1}, 1\pi^{-1}$ $4\sigma^{-1}$		
12.7	$5\sigma^{-1}\text{CT}^c$ $1\pi^{-1}\text{CT}^c$	389 (13.6) ^b (14.7) ^a	$5\sigma^{-1}\text{CT}^c$ ($5\sigma^{-1}\text{CT}^c$) ^b ($1\pi^{-1}\text{CT}^c$) ^b ($4\sigma^{-1}\text{CT}^c$) ^b
16.8	$4\sigma^{-1}\text{CT}^c$		
19.9	$1\pi^{-2}\pi^*$ $1\pi^{-1}1\pi^{-1}\pi^*$ $5\sigma^{-1}1\pi^{-1}\pi^*$	(19.7) ^b	($1\pi^{-2}\pi^*$) ^b ($5\sigma^{-2}\pi^*$) ^b ($5\sigma^{-1}1\pi^{-1}\pi^*$) ^b
24.2	$4\sigma^{-1}1\pi^{-1}\pi^*$	379	$4\sigma^{-1}1\pi^{-1}\pi^*$
26.5	$4\sigma^{-1}1\pi^{-1}\pi^*$		

^a With reference to E_f . ^b Values in brackets are due to CO/Pd(100). ^c CT means decay with metal orbital taking part. ^d Ref. [33].

variations of the relative autoionization probability which describes the most important features of the spectrum. In Table 3 an overview of recent assignments is given. They are very similar to the presented ones.

It is now appropriate to compare the results presented with those on the autoionization of CO on a Ni(110) surface [26,32]. CO is isoelectronic to N_2 having the same occupied orbitals. In addition, the excited state of the $\text{C}1s \rightarrow \pi^*$ and the excitation of the outer nitrogen atom are the same in the equivalent core approximation. At first glance the spectra are very similar. The feature at lowest energy is governed by single hole states. The calculated intensity is too high, independently of whether ab initio or semiempirical wave functions are used for CO as in the present case. The second feature, which is the first intense one, is governed by charge transfer states in both cases. The third peak is the strongest for CO and for N_2 , and the intensity originates from states of the $(1\pi^{-1}1\pi^{-1}\pi^*)^1$ type. The tailing of the main peak is governed by $(4\sigma^{-1}1\pi^{-1}\pi^*)^1$ states. The same is true for the following small peak situated at about 28 eV in the CO case. In the N_2 case this peak is hidden in the broader structure. This is revealed by looking at the spectra of the different nitrogen atoms (Figs. 4 and 5). The spectrum of the outer

nitrogen is very similar to that of CO after $\text{C}1s \rightarrow \pi^*$ excitation for the reasons discussed before. This can be seen in the data of Björneholm et al. [33] as well as in the calculated spectra presented in this paper. The angular dependence of the peaks may be understood on the same basis. The first peak in the N_2 spectra exhibits similar behavior to that of the first peak of the CO data after $\text{C}1s \rightarrow \pi^*$ excitation. Its intensity stems from the outer nitrogen atom as discussed before. The same is true for the CT peak near in energy. It is nearly missing in the spectrum of the inner nitrogen atom. The angular dependence of the spectra is the same as that measured after $\text{C}1s \rightarrow \pi^*$ excitation of CO. A comparably good agreement has been found for the third peak. The fourth peak, the main peak of the spectrum, is strong for both nitrogen atoms as well as after $\text{C}1s \rightarrow \pi^*$ or after $\text{O}1s \rightarrow \pi^*$ excitation of CO. Also the angular dependences are similar. The fifth feature originating from $(4\sigma^{-1}1\pi^{-1}\pi^*)^1$ states is stronger in the spectrum of the inner nitrogen atom and the angular dependence is similar to that of CO after $\text{O}1s \rightarrow \pi^*$ excitation. These states are responsible for the broadening of the main peak. Summarizing, we find that the similarity of the autoionization of CO and N_2 is very pronounced. Even the angular dependences of both systems are comparable. Perhaps, after all, this is not too surprising because the systems are isoelectronic, but it is rewarding to see it reproduced in experiment and theory.

5. Summary and conclusions

In the present work, autoionization spectra of nitrogen on a Ni(110) surface are presented together with an assignment of features in the spectra by means of a CNDO Green's functions calculation. The autoionization spectra have been recorded as a function of the polar angle, and the experimentally observed angular dependences are compared with theoretical predictions.

The calculated autoionization spectra are in line with those observed experimentally. There is also agreement with experimental data from the Uppsala group [33] where it was possible to

resolve the spectra of the two chemically different nitrogen atoms.

A comparison with a corresponding set of calculations for CO on the same surface indicates the similarities expected for these two isoelectronic systems, emphasizing the difference between the autoionization process of molecules in the gas phase and autoionization of molecules on metallic surfaces.

Acknowledgments

The present work was financially supported in part by the "Bundesministerium für Forschung und Technologie" under project No. 05 432 FAB0. The "Höchstleistungsrechenzentrum der KFA Jülich" is gratefully acknowledged for providing the necessary computer time on their Cray Y-MP computer. J.K. thanks the Graduiertenkolleg "Dynamische Prozesse an Festkörperoberflächen" for financial support.

References

- [1] W. Unertl, M. Golze and M. Grunze, *Prog. Surf. Sci.*, 22 (1986) 101.
- [2] M. Grunze, R.K. Driscoll, G.N. Burland, J.C.L. Cornish and J. Pritchard, *Surf. Sci.*, 89 (1979) 381.
- [3] W.N. Unertl, M. Grunze, P.H. Kleban and F.S. Rys, *Phys. Rev. Lett.*, 51 (1983) 582.
- [4] M. Onchi, Y. Kuwahara, M. Fujisawa and M. Nishijima, *Surf. Sci.*, 207 (1988) 17.
- [5] C.R. Brundle, P.S. Bagus, D. Menzel and K. Hermann, *Phys. Rev. B*, 24 (1981) 7041.
- [6] K. Hermann, P.S. Bagus, C.R. Brundle and D. Menzel, *Phys. Rev. B*, 24 (1981) 7025.
- [7] R.K. Driscoll, M. Golze, M. Grunze and W. Hirsch, *Appl. Surf. Sci.*, 6 (1980) 464.
- [8] Y.-P. Hsu, K. Jacobi and H.H. Rotermund, *Surf. Sci.*, 117 (1982) 581.
- [9] K. Jacobi and H.H. Rotermund, *Surf. Sci.*, 133 (1983) 401.
- [10] K. Horn, J. DiNardo, W. Eberhardt, H.-J. Freund and E.W. Plummer, *Surf. Sci.*, 118 (1982) 465.
- [11] T. Koopmans, *Physica*, 1 (1932/1933) 104.
- [12] W. Domcke, J. Schirmer, L.S. Cederbaum and W. von Niessen, *Chem. Phys.*, 26 (1977) 149.
- [13] W. Domcke, L.S. Cederbaum, J. Schirmer and W. von Niessen, *J. Phys. B*, 10 (1977) L549.
- [14] L.S. Cederbaum and W. Domcke, *Adv. Chem. Phys.*, 36 (1977) 205.
- [15] L.S. Cederbaum, W. Domcke, J. Schirmer and W. von Niessen, *Adv. Chem. Phys.*, 65 (1986) 115.
- [16] D. Saddei, H.-J. Freund and G. Hohlneicher, *Surf. Sci.*, 95 (1980) 527.
- [17] D. Saddei, Ph.D. thesis, Universität Köln, 1982.
- [18] J. Schirmer and L.S. Cederbaum, *J. Phys. B*, 11 (1978) 1889.
- [19] M. Ohno and W. von Niessen, *Phys. Rev. B*, 42 (1990) 7370.
- [20] M. Ohno and W. von Niessen, *Phys. Rev. B*, 44 (1991) 1896.
- [21] A.I.H. Wachters, *J. Chem. Phys.*, 52 (1970) 1033.
- [22] A. Veillard and C. Salez, *Theor. Chim. Acta*, 11 (1968) 441.
- [23] N. Sauerwald, Diplomarbeit, Ruhr-Universität Bochum, 1992.
- [24] T.N. Rhodin, P.A. Dowben and Y. Sakisaka, *Surf. Sci.*, 147 (1984) 89.
- [25] C.-M. Liegener, T. Porwol, G. Illing, H.-J. Freund, H. Kuhlenbeck, M. Neumann, S. Bernstorff, W. Braun and W. von Niessen, *Phys. Rev. B*, 41 (1990) 10510.
- [26] T. Porwol, Ph.D. thesis, Ruhr-Universität Bochum, 1992.
- [27] G. Illing, T. Porwol, I. Hemmerich, G. Dömötör, H. Kuhlenbeck, H.-J. Freund, C.-M. Liegener and W. von Niessen, *J. Electron Spectrosc. Relat. Phenom.*, 51 (1990) 149.
- [28] H. Siegbahn, L. Asplund and P. Kelfve, *Chem. Phys. Lett.*, 35 (1975) 330.
- [29] E.J. McGuire, *Phys. Rev.*, 185 (1969) 1.
- [30] E.J. McGuire, Sandia Laboratories Res. Rep. SC-RR-69-137, 1969.
- [31] J. Cooper and R.N. Zare, in S. Geltman, K.T. Mahanthappa and W.E. Brittin (Eds.), *Photoelectron angular distributions, in Theoretical Physics, Vol. 11c*, Gordon and Breach, New York, 1969, p. 317.
- [32] T. Porwol, G. Dömötör, I. Hemmerich, J. Klinkmann, H.-J. Freund and C.-M. Liegener, *Phys. Rev. B*, 49 (1994) 10557.
- [33] O. Björneholm, A. Sandell, A. Nilsson, N. Mårtensson and J.N. Anderson, *Phys. Scr. T*, 41 (1992) 217.
- [34] O. Björneholm, A. Sandell, A. Nielsen, E.O.F. Zdansky, H. Tillborg, J.N. Andersen and N. Mårtensson, *Phys. Rev. Lett.*, 70 (1993) 2000.
- [35] O. Björneholm, Ph.D. Thesis, Uppsala University, 1992.
- [36] E. Umbach and Z. Hussain, *Phys. Rev. Lett.*, 52 (1984) 754.
- [37] P. Maciejewski, U. Höfer, W. Wurth and E. Umbach, *J. Electron Spectrosc. Relat. Phenom.*, 62 (1993) 1.
- [37] Berliner Elektronenspeichering-Gesellschaft für Synchrotronstrahlung m.b.H., Lentzeallee 100, 14195 Berlin.